NEAR-FIELD IMAGING OF INFINITE ROUGH SURFACES

GANG BAO* AND PEIJUN LI†

Abstract. This paper is concerned with an inverse rough surface scattering problem in near-field optical imaging, which is to reconstruct the scattering surface with a resolution beyond the diffraction limit. The surface is assumed to be a small and smooth deformation of a plane surface. Based on a transformed field expansion, the boundary value problem with complex scattering surface is converted into a successive sequence of a two-point boundary value problems in the frequency domain, where an analytic solution for the direct scattering problem is derived from the method of integrated solution. By neglecting the high order terms in the power series expansion, the nonlinear inverse problem is linearized and an explicit inversion formula is obtained. A spectral cut-off regularization is adopted to suppress the exponential growth of the noise in the evanescent wave components, which carry high spatial frequency of the scattering surface and contribute to the super resolution in the near-field regime. The method works for sound soft, sound hard, and impedance surfaces, and requires only a single illumination at a fixed frequency and is realized efficiently by the fast Fourier transform. Numerical results show that the method is simple, stable, and effective to reconstruct scattering surfaces with subwavelength resolution.

Key words. inverse scattering, transformed field expansion, near-field imaging, Helmholtz equation

AMS subject classifications. 65N21, 78A46

1. Introduction. Scattering problems are concerned with how an inhomogeneous medium scatters an incident field. The direct scattering problem is to determine the scattered field from the incident field and the differential equation governing the wave motion; the inverse scattering problem is to determine the nature of the inhomogeneity, such as geometry and material property, from the measured scattered field (cf. Colton and Kress [17]). These problems have played a fundamental role in diverse scientific areas such as radar and sonar (e.g., submarine detection), geophysical exploration (e.g., oil and gas exploration), and medical imaging (e.g., breast cancer detection). However, there is a resolution limit to the sharpness of details that can be observed by conventional far-field optical microscopy, one half the wavelength, referred to as the Rayleigh criterion or the diffraction limit (cf. Courjon and Bainier [19]). Near-field optical imaging is an effective approach to breaking the diffraction limit and obtaining images with subwavelength resolution (cf. Courjon [18]), which leads to exciting applications in broad areas of modern science and technology, including surface chemistry (e.g., detection and spectroscopy of single molecules), biology (e.g., imaging of single proteins and photosynthetic membranes), materials science (e.g., self-luminous device and waveguide), and information storage (e.g., magneto-optics data storage). This paper is aimed to develop an effective mathematical model and design an efficient computational method for solving the surface scattering problem that arises in near-field optical imaging.

We study the scattering by a surface with the impedance boundary condition,

*Department of Mathematics, Zhejiang University, Hangzhou 310027, China; Department of Mathematics, Michigan State University, East Lansing, Michigan 48824, USA (drbaogang@gmail.com). The research was supported in part by the NSF grants DMS-0908325, DMS-0968360, DMS-1211292, the ONR grant N00014-12-1-0319, a Key Project of the Major Research Plan of NSFC (No. 91130004), and a special research grant from Zhejiang University..

†Department of Mathematics, Purdue University, West Lafayette, Indiana 47907, USA (lipeijun@math.purdue.edu). The research was supported in part by the NSF grants DMS-1042958 and DMS-1151308.

which includes the sound soft and the sound hard boundary conditions. The wave motion is governed by the two-dimensional Helmholtz equation, which describes the propagation of acoustic waves or the transverse magnetic polarization of electromagnetic waves. Specifically, we consider the scattering of a time-harmonic plane wave incident on an impedance scattering surface from the top, where the space above the scattering surface is filled with some homogeneous medium. The impedance boundary condition is not essential for the scattering surface; it actually reduces to the sound soft or perfect electric conductor and the sound hard boundary conditions depending on the impedance constant. The method can be naturally extended to solve the transmission problem, where the wave can penetrate the medium, and the electromagnetic surface scattering problem, which will be reported in future work. In the applications of near-field imaging, it is reasonable to assume that the scattering surface is a small and smooth deformation of a plane surface. The deformation is allowed to be very general: it could be a non-local perturbation of a plane surface, which is referred to as an infinite or unbounded rough surface (cf. Voronovich [36], Warnick and Chew [37]); it could be a local perturbation of a plane surface, which is called cavity wall (cf. Jin [24]) when the perturbed surface is below the plane surface; or it could be of a periodic structure, which is known as a grating surface (cf. Bao, Cowsar, and Masters [3]). Given the scattering surface and a time-harmonic plane incident wave, the direct scattering problem is to predict the wave field distribution away from the surface. We are mainly interested in studying the inverse scattering problem: what information can we extract about the surface from the wave field measured at a constant distance above the scattering surface, particularly in the near-field regime, i.e., at a distance which is much smaller than the wavelength of the incident wave.

The direct problem has been examined extensively by numerous researchers via either integral equation methods or variational approaches in aforementioned three modalities, such as the infinite or unbounded rough surface scattering by Chandler-Wilde and Monk [12], DeSanto and Martin [20], Li, Wu, and Zheng [28], Milder [32], Zhang and Chandler-Wilde [38, 39]; the cavity scattering problem by Ammari, Bao, and Wood [1], Bao, Gao, and Li [5], Li and Wood [27]; the diffraction grating problem by Bao, Dobson, and Cox [4], and references cited therein. The inverse problem has also been investigated widely for these modalities, such as Akduman, Kress, and Yaper [2], Coifman et al. [16], DeSanto and Wombell [21], Lines and Chandler-Wilde [27], Kress and Tran [25], Bao, Li, and Wu [6], Bao, Li, Lv [7], and references therein. These work addressed conventional far-field imaging, where the role of evanescent wave components were ignored and the resolution of reconstructions were limited by the Rayleigh criterion. As shown experimentally (cf. Girard and Dereux [23]), a light beam illuminating on a sample characterized by a fine structure will be converted into propagating components, which are able to propagate towards the remote detector, and evanescent components, which are confined on the surface. The first ones are associated to the low spatial frequencies of the sample whereas the second ones are connected to their high frequencies, which do not obey the Rayleigh criterion and contribute to the subwavelength resolution. However, it is severely ill-posed to directly make use of the evanescent waves since the noise in the measurements is amplified exponentially and all the useful information is covered by it. Thus, it is important to consider a regularization technique to suppress the exponential growth of the noise in the evanescent wave components. A trade-off is necessary between the resolution and the signal-to-noise ratio (SNR) of the data in order to obtain a stable and super resolved reconstruction.

In this paper, we consider a rigorous mathematical model for a class of surface scattering problems in near-field optical imaging. The model problem is formulated as a boundary value problem for the two-dimensional Helmholtz equation with a transparent boundary condition proposed on a plane surface confining the scattering surface. Based on a transformed field expansion, the boundary value problem with complex scattering surface is reduced into a successive sequence of the Helmholtz equation with a plane surface. The reduced problem is further converted into a two-point boundary value problem in the frequency domain and is solved analytically by the method of integration solution. For transformed field expansion method and related boundary perturbation method, we refer to the work by Nicholls and Reitich [33, 34], Bruno and Reitich [9], Malcolm and Nicholls [30], and Li and Shen [26] for solving the direct diffraction grating problem and the direct unbounded rough surface scattering problem, respectively. A boundary perturbation method may be found in Malcolm and Nicholls [31] for solving a inverse scattering problem with a periodic surface. By neglecting the high order terms in the power series expansion for the analytical solution, the nonlinear inverse problem is linearized, and an explicit inversion formula is obtained. The inversion method is valid for surfaces with the sound soft, sound hard, and impedance boundary conditions. It requires only a single illumination of a plane wave, particularly the normal incidence, at a fixed frequency, and can be done efficiently by the fast Fourier transform (FFT). Spectral cut-off regularization is adopted to suppress the exponential growth of the evanescent wave modes. Results show that the method is simple, stable, and effective to reconstruct scattering surfaces with subwavelength resolution.

We point out a closely related work on the inverse surface scattering in near-field imaging by Bao and Lin [8], where the scattering surface is assumed to be a perfect electric conductor and a local perturbation of a plane surface. Due to a locally perturbed surface, the usual Sommerfeld radiation condition is imposed for the scattered field in their model problem. We consider a general scattering surface with either sound soft, sound hard, or impedance boundary condition. In addition, the Sommerfeld radiation condition may no longer be valid for the case of a nonlocal perturbation of a plane surface, such as for the unbounded rough surface scattering problem and the diffraction grating problem. An appropriate transparent boundary condition needs to be imposed for our model problem. We give a more rigorous argument for the linearization procedure and the dependence of the resolution on the parameters of the deformation parameter, measurement distance, and noise level. Another related work may be found in Carney and Schotland [10, 11] for solving an inverse medium scattering problem in near-field optical imaging.

The outline of this paper is as follows. In Section 2, a mathematical model is introduced and formulated into a boundary value problem by using a transparent boundary condition. A transformed field expansion is presented to analytically derive the solution for the direct surface scattering problem in Section 3. Section 4 is devoted to derivation of an explicit inversion formula for the inverse surface scattering problem. In Section 5, numerical implementations are discussed and numerical examples are reported to demonstrate the effectiveness of the proposed method. The paper is concluded with some general remarks and directions for future research in Section 6.

2. A model problem. In this section, we shall introduce a mathematical model, define some notations for the scattering problem by a surface, and present a boundary value problem for the surface scattering model.

As seen in Figure 2.1, let the scattering surface be described by the curve $S =$

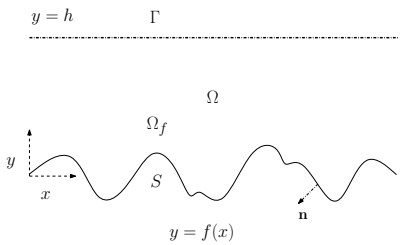

FIG. 2.1. *Problem geometry. A plane wave is incident on the scattering surface S from the top. The space Ω_f above S is filled with a homogeneous medium with positive constant wavenumber κ.*

$\{(x, y) \in \mathbb{R}^2 : y = f(x),\ x \in \mathbb{R}\}$, where the function f is assumed to be in the form

$$f(x) = \varepsilon g(x), \quad g \in C^2(\mathbb{R}) \tag{2.1}$$

with a sufficiently small surface deformation parameter ε. So we assume that the scattering surface is a sufficiently small and smooth deformation of a plane surface. The deformation is not restricted to a local perturbation of a plane surface but considered to be rather general including nonlocal perturbation of a plane surface.

Let the space above the scattering surface $\Omega_f = \{(x, y) \in \mathbb{R}^2 : y > f(x),\ x \in \mathbb{R}\}$ be filled with a homogeneous medium with positive constant wavenumber κ. The associated wavelength is $\lambda = 2\pi/\kappa$. Denote by Ω the domain bounded below by the scattering surface S and bounded above by the line $\Gamma = \{(x, y) \in \mathbb{R}^2 : y = h,\ x \in \mathbb{R}\}$, i.e.,

$$\Omega = \{(x, y) \in \mathbb{R}^2 : f(x) < y < h,\ x \in \mathbb{R}\}.$$

In the context of the inverse problem, the wave field is measured on the line Γ. So h stands for the measurement distance to the scattering surface.

Let an incoming plane wave $u^{\text{inc}}(x, y) = e^{\mathrm{i}(\alpha x - \beta y)}$ be incident on the scattering surface from above, where $\alpha = \kappa \sin\theta, \beta = \kappa \cos\theta,\ \theta \in (-\pi/2, \pi/2)$ is the angle of incidence with respect to the positive y-axis. For normal incidence, i.e., $\theta = 0$, we have $\alpha = 0$ and $\beta = \kappa$. The incident field reduces to $u^{\text{inc}}(x, y) = e^{-\mathrm{i}\kappa y}$. We will particularly focus on the case of normal incidence when deriving the inversion formula to reconstruct the scattering surface. It can be verified that the incident wave satisfies the Helmholtz equation in the whole space

$$\Delta u^{\text{inc}} + \kappa^2 u^{\text{inc}} = 0 \quad \text{in } \mathbb{R}^2. \tag{2.2}$$

The scattering of an plane wave by an unbounded rough surface can be modeled by the two-dimensional Helmholtz equation:

$$\Delta u + \kappa^2 u = 0 \quad \text{in } \Omega_f. \tag{2.3}$$

For the sound soft or the perfect electric conductor boundary condition, the total field u vanishes on the scattering surface S:

$$u = 0 \quad \text{on } S. \tag{2.4}$$

For the sound hard boundary condition, the normal derivative of the total field $\partial_{\mathbf{n}} u$ vanishes on the scattering surface S:

$$\partial_{\mathbf{n}} u = 0 \quad \text{on } S, \tag{2.5}$$

where $\mathbf{n} = (n_1, n_2)^\top$ is the unit outward normal vector on S, given explicitly as

$$n_1 = \frac{f'(x)}{\sqrt{1+[f'(x)]^2}} \quad \text{and} \quad n_2 = -\frac{1}{\sqrt{1+[f'(x)]^2}}. \tag{2.6}$$

For the impedance boundary condition, the total field satisfies

$$\partial_{\mathbf{n}} u + \nu u = 0 \quad \text{on } S, \tag{2.7}$$

where $\nu \in \mathbb{C}$ is the impedance coefficient and is assumed $\mathrm{Re}\nu \neq 0$ and $\mathrm{Im}\nu \neq 0$, which assures the unique solvability of the direct problem. Clearly, the impedance boundary condition (2.7) reduces to the sound hard boundary condition (2.5) when $\nu = 0$, and reduces to the sound soft boundary condition (2.4) when $\nu = \infty$. Throughout, we shall use the impedance boundary condition (2.7) to present the model problem and the results are applicable to the sound soft and the sound hard boundary conditions.

Due to the interaction between the incident field and the scattering surface, the total field u is composed of the incident field u^{inc} and the scattered field u^{s}:

$$u = u^{\mathrm{inc}} + u^{\mathrm{s}}.$$

For the surface scattering problem, the usual Sommerfeld radiation condition may not be valid for the scattered field. We impose the outgoing wave condition: the scattered field consists of bounded outgoing waves. We refer to Chandler-Wilde and Zhang [13], and Chandler-Wilde, Ross, and Zhang [14] for study of the unbounded rough surface scattering problem with a Dirichlet or an impedance boundary condition by introducing an upward propagating radiation condition.

Next we introduce a transparent boundary condition on Γ, which is equivalent to the outgoing wave condition. Given u, the Fourier transform of u is defined by

$$\hat{u}(\xi) = (2\pi)^{-1/2} \int_{\mathbb{R}} u(x) e^{-\mathrm{i}\xi x} dx.$$

It follows from (2.2) and (2.3) that the scattered field satisfies

$$\Delta u^{\mathrm{s}} + \kappa^2 u^{\mathrm{s}} = 0 \quad \text{for } y > h. \tag{2.8}$$

By taking the Fourier transform of (2.8) with respect to x, we have

$$\frac{\partial^2 \hat{u}^{\mathrm{s}}(\xi, y)}{\partial y^2} + (\kappa^2 - \xi^2)\hat{u}^{\mathrm{s}}(\xi, y) = 0 \quad \text{for } y > h. \tag{2.9}$$

Noting the outgoing wave condition for the scattered field, we may deduce that the solution of (2.9) is given by

$$\hat{u}^{\mathrm{s}}(\xi, y) = \hat{u}^{\mathrm{s}}(\xi, h) e^{\mathrm{i}\eta(y-h)}, \tag{2.10}$$

where

$$\eta(\xi) = \begin{cases} (\kappa^2 - \xi^2)^{1/2} & \text{for} \quad |\xi| < \kappa, \\ \mathrm{i}(\xi^2 - \kappa^2)^{1/2} & \text{for} \quad |\xi| > \kappa. \end{cases} \tag{2.11}$$

Taking the inverse Fourier transform on both sides of (2.10), we have

$$u^{\mathrm{s}}(x, y) = (2\pi)^{-1/2} \int_{\mathbb{R}} \hat{u}^{\mathrm{s}}(\xi, h) e^{\mathrm{i}\eta(y-h)} e^{\mathrm{i}\xi x} d\xi.$$

Taking the partial derivative with respect to y and then evaluating at $y = h$ on both sides of the above equation yield

$$\partial_y u^{\mathrm{s}}(x,h) = (2\pi)^{-1/2} \int_{\mathbb{R}} \mathrm{i}\eta \hat{u}^{\mathrm{s}}(\xi,h) e^{\mathrm{i}\xi x} d\xi.$$

For any given u on Γ, i.e., $u(x,h)$, we define the boundary operator T:

$$Tu = (2\pi)^{-1/2} \int_{\mathbb{R}} \mathrm{i}\eta(\xi) \hat{u}(\xi,h) e^{\mathrm{i}\xi x} d\xi,$$

which maps the Dirichlet data $u(x,h)$ to the Neumann data $\partial_y u(x,h)$. A transparent boundary condition on Γ can be written as

$$\partial_y (u - u^{\mathrm{inc}}) = T(u - u^{\mathrm{inc}}).$$

Equivalently, this transparent boundary condition can be reformulated as

$$\partial_y u = Tu + \rho \quad \text{on } \Gamma, \tag{2.12}$$

where

$$\rho = \partial_y u^{\mathrm{inc}} - Tu^{\mathrm{inc}}.$$

More explicitly, it can be verified from the incident field and the boundary operator that

$$\rho = -2\mathrm{i}\beta e^{\mathrm{i}(\alpha x - \beta h)}. \tag{2.13}$$

To summarize, the surface scattering model can be reduced to the following boundary value problem for the total field:

$$\begin{aligned} \Delta u + \kappa^2 u &= 0 \quad \text{in } \Omega, \\ \partial_{\mathbf{n}} u + \nu u &= 0 \quad \text{on } S, \\ \partial_y u &= Tu + \rho \quad \text{on } \Gamma. \end{aligned} \tag{2.14}$$

There are two problems to be solved, the direct surface scattering problem and the inverse surface scattering problem. The direct problem is to determine the total field u, given the incident field u^{inc} and the scattering surface function f. This paper is focused on the inverse surface scattering problem, which is to reconstruct the scattering surface function f from the measurement of the total field u, given the incident field u^{inc}. More specifically, this work is to reconstruct the function $f(x)$ from noisy data of the total field measured at Γ, i.e., $u^\delta(x,h)$, corresponding to a fixed wavenumber κ and a single incident direction θ, where δ is the noise level for the measurement. In particular, we are interested in the inverse scattering in near-field regime where the measurement distance h is much smaller than the wavelength λ, i.e., $h \ll \lambda$.

We point out that the scattering solution u is only bounded and continuous in the setting of this work, i.e., scattering of a time-harmonic plane wave by an unbounded rough surface in a homogeneous medium with $\kappa > 0$. The Fourier transform is only taken in the sense of a tempered distribution, and the boundary operator T may not be well defined in a regular Sobolev space. To overcome this difficulty, we may use the limiting absorption principle, i.e., replace κ^2 by $\kappa^2 + \mathrm{i}\gamma$ with $\gamma > 0$ being small, to get a solution u_γ, which is in $H^1(\Omega)$ and its restriction on Γ is in $H^{1/2}(\Gamma)$. The Fourier transform can be taken in the usual sense of $L^2(\Gamma)$, which is identified with $L^2(\mathbb{R})$. It was also shown in Li and Shen [26] that T is bounded from $H^{1/2}(\Gamma)$ to $H^{-1/2}(\Gamma)$. The original solution u is then defined by the limit $\lim_{\gamma \to 0} u_\gamma(x,y) = u(x,y)$ for any (x,y) in the domain.

3. Transformed field expansion. In this section, we introduce the transformed field expansion to analytically derive the solution for the direct surface scattering problem (2.14). The expansion of the solution is given as a power series of the parameter ε and plays an important role for our inversion formula.

The transformed field expansion method begins with the change of variables:

$$\tilde{x} = x, \quad \tilde{y} = h\left(\frac{y-f}{h-f}\right),$$

which maps the domain Ω with a complex scattering surface S to the strip

$$D = \{(\tilde{x}, \tilde{y}) \in \mathbb{R}^2 : 0 < \tilde{y} < h\} = \mathbb{R} \times (0,\ h)$$

with a plane surface $y = 0$.

We seek to restate the surface scattering problem (2.14) in this transformed coordinate. It is easy to verify the differentiation rules

$$\begin{aligned}\partial_x &= \partial_{\tilde{x}} - f'\left(\frac{h-\tilde{y}}{h-f}\right)\partial_{\tilde{y}},\\ \partial_y &= \left(\frac{h}{h-f}\right)\partial_{\tilde{y}}.\end{aligned}$$

Introduce a new function $w(\tilde{x}, \tilde{y}) = u(x, y)$ under the transformation. It can be verified after tedious but straightforward calculations from (2.3) that w, upon dropping the tilde, satisfies the equation

$$c_1\frac{\partial^2 w}{\partial x^2} + c_2\frac{\partial^2 w}{\partial y^2} + c_3\frac{\partial^2 w}{\partial x \partial y} + c_4\frac{\partial w}{\partial y} + c_1\kappa^2 w = 0 \quad \text{in } D, \tag{3.1}$$

where

$$\begin{aligned}c_1 &= (h-f)^2,\\ c_2 &= [f'(h-y)]^2 + h^2,\\ c_3 &= -2f'(h-y)(h-f),\\ c_4 &= -(h-y)[f''(h-f) + 2(f')^2].\end{aligned}$$

Under the change of variables, the impedance boundary condition (2.7) becomes

$$n_1\left(1-\frac{f}{h}\right)\partial_x w + (n_2 - n_1 f')\partial_y w + \nu\left(1-\frac{f}{h}\right)w = 0 \quad \text{on } y = 0. \tag{3.2}$$

Plugging (2.6) into (3.2), we have

$$f'\left(1-\frac{f}{h}\right)\partial_x w - \left(1+(f')^2\right)\partial_y w + \nu\left(1+(f')^2\right)^{1/2}\left(1-\frac{f}{h}\right)w = 0. \tag{3.3}$$

The transparent boundary condition (2.12) reduces to

$$\partial_y w = \left(1-\frac{f}{h}\right)(Tw + \rho) \quad \text{on } y = h. \tag{3.4}$$

Recalling the surface scattering function $f = \varepsilon g$ in (2.1), we use a classical boundary perturbation argument and consider the formal expansion of w in a power series of ε:

$$w(x, y; \varepsilon) = \sum_{n=0}^{\infty} w_n(x, y)\, \varepsilon^n. \tag{3.5}$$

Substituting $f = \varepsilon g$ into c_j and inserting the power series expansion (3.5) into (3.1), we may derive the recursion for w_n:

$$\frac{\partial^2 w_n}{\partial x^2} + \frac{\partial^2 w_n}{\partial y^2} + \kappa^2 w_n = v_n \quad \text{in } D, \tag{3.6}$$

where

$$\begin{aligned} v_n =& \frac{2g}{h}\frac{\partial^2 w_{n-1}}{\partial x^2} + \frac{2g'(h-y)}{h}\frac{\partial^2 w_{n-1}}{\partial x \partial y} + \frac{g''(h-y)}{h}\frac{\partial w_{n-1}}{\partial y} + \frac{2\kappa^2 g}{h} w_{n-1} \\ & - \frac{g^2}{h^2}\frac{\partial^2 w_{n-2}}{\partial x^2} - \frac{(g')^2(h-y)^2}{h^2}\frac{\partial^2 w_{n-2}}{\partial y^2} - \frac{2gg'(h-y)}{h^2}\frac{\partial^2 w_{n-2}}{\partial x \partial y} \\ & + \frac{[2(g')^2 - gg''](h-y)}{h^2}\frac{\partial w_{n-2}}{\partial y} - \frac{\kappa^2 g^2}{h^2} w_{n-2}. \end{aligned} \tag{3.7}$$

The impedance boundary condition (3.3) can be written as

$$\partial_y w_n - \nu w_n = \phi_n \quad \text{on } y = 0, \tag{3.8}$$

where

$$\begin{aligned} \phi_n =& g'\partial_x w_{n-1} - \nu\left(\frac{g}{h}\right) w_{n-1} - g'\left(\frac{g}{h}\right)\partial_x w_{n-2} - (g')^2 \partial_y w_{n-2} \\ & + \nu \sum_{k=1}^{\lfloor \frac{n}{2} \rfloor} \begin{pmatrix} \frac{1}{2} \\ k \end{pmatrix} (g')^{2k} \left[w_{n-2k} - \left(\frac{g}{h}\right) w_{n-2k-1} \right]. \end{aligned} \tag{3.9}$$

Here $\lfloor n \rfloor$ is the largest integer not greater than n and the generalized binomial coefficient

$$\begin{pmatrix} \frac{1}{2} \\ k \end{pmatrix} = \frac{\frac{1}{2}(\frac{1}{2}-1)\cdots(\frac{1}{2}-k+1)}{k!}.$$

The transparent boundary condition (3.4) reduces to

$$\partial_y w_n - T w_n = \psi_n \quad \text{on } y = h, \tag{3.10}$$

where

$$\psi_0 = \rho, \quad \psi_1 = -\left(\frac{g}{h}\right)(T w_0 + \rho), \quad \psi_n = -\left(\frac{g}{h}\right) T w_{n-1}, \quad n = 2, 3, \ldots. \tag{3.11}$$

In all of the above recursions, it is understood that w_n, v_n, ϕ_n, ψ_n are zeros when $n < 0$. Note that the transformed scattering problem (3.6)–(3.10) for the current term w_n involves nonhomogeneous terms v_n and ρ_n, which depend on previous terms $w_{n-1}, w_{n-2}, \ldots, w_0$. Thus, the transformed scattering problem (3.6)–(3.10) indeed can be solved in a recursive manner starting from $n = 0$.

Next we derive an analytical solution for the transformed scattering problem (3.6) together with the boundary conditions (3.8) and (3.10). Taking the Fourier transform of (3.6) with respect to the variable x, we obtain a second order ordinary differential equation

$$\frac{\partial^2 \hat{w}_n}{\partial y^2} + \eta^2 \hat{w}_n = \hat{v}_n, \quad 0 < y < h, \tag{3.12}$$

where η is defined in (2.11). Under the Fourier transform, the impedance boundary condition (3.8) becomes

$$\partial_y \hat{w}_n - \nu \hat{w}_n = \hat{\phi}_n \quad \text{on } y = 0. \tag{3.13}$$

Importantly, the nonlocal transparent boundary condition (3.10) becomes a local boundary condition in the frequency domain:

$$\partial_y \hat{w}_n - \mathrm{i}\eta \hat{w}_n = \hat{\psi}_n \quad \text{on } y = h. \tag{3.14}$$

After taking the Fourier transform, the two-dimensional scattering problem for the Helmholtz equation (3.6), (3.8), (3.10) reduces to a one-dimensional two-point boundary value problem (3.12)–(3.14) in the frequency domain, which can be solved analytically. Note that η is either a real number or pure imaginary number, thus $\nu \neq \mathrm{i}\eta$ for all $\xi \in \mathbb{R}$. Using Theorem B.1, we may obtain an explicit solution of the two-point boundary value problem (3.12)–(3.14).

THEOREM 3.1. *The two-point boundary value problem* (3.12)–(3.14) *has a unique solution, which is given explicitly as*

$$\hat{w}_n(\xi, y) = K_1(\xi, y)\hat{\phi}_n(\xi) - K_2(\xi, y)\hat{\psi}_n(\xi) + \int_0^h K_3(\xi, y, z)\hat{v}_n(\xi, z)dz, \tag{3.15}$$

where

$$K_1(\xi, y) = \frac{e^{\mathrm{i}\eta y}}{\mathrm{i}\eta - \nu}, \quad K_2(\xi, y) = \frac{e^{\mathrm{i}\eta(h-y)}}{\mathrm{i}\eta - \nu} K(\xi, y),$$

and

$$K_3(\xi, y, z) = \begin{cases} \dfrac{e^{\mathrm{i}\eta(y-z)}}{\mathrm{i}\eta - \nu} K(\xi, z), & z < y, \\ \dfrac{e^{\mathrm{i}\eta(z-y)}}{\mathrm{i}\eta - \nu} K(\xi, y), & z > y. \end{cases}$$

Here

$$K(\xi, t) = \frac{(\eta + \mathrm{i}\nu)}{2\eta} + \frac{(\eta - \mathrm{i}\nu)}{2\eta} e^{2\mathrm{i}\eta t}.$$

It follows from Theorem 3.1 that the power series expansion (3.5) along with the solution representation (3.15) for the two-point boundary value problem (3.12)–(3.14) explicitly gives an analytical solution of the surface scattering problem (2.14) for the scattering surface given in (2.1). It may be seen from the definitions of K_j and the solution representation (3.15) that the spatial frequency $|\xi| < \kappa$ accounts for

the propagation wave components, which propagate in both the x and y directions, while the spatial frequency $|\xi| > \kappa$ stands for the evanescent wave components, which propagate in the x direction and decay exponentially in the y direction.

REMARK 3.2. *Under the assumption that f has two continuous derivatives, i.e., $f \in C(\mathbb{R})$, we may follow the same techniques by Nicholls and Reitich in [33] to show inductively that the power series for w in* (3.5) *converges for sufficiently small ε.*

4. Reconstruction formula. Based on the transformed field expansion, we present an efficient and stable method to reconstruct the scattering surface f from the noisy data of the total field $u^\delta(x,h)$, which is assumed to take the form

$$u^\delta(x,h) = u(x,h) + O(\delta). \tag{4.1}$$

Here $u(x,h)$ denotes the noise free data and δ represents the noise level.

It follows from the power series expansion (3.5) that we have

$$w(x,y) = w_0(x,y) + \varepsilon w_1(x,y) + O(\varepsilon^2), \tag{4.2}$$

where ε is the surface deformation parameter introduced in (2.1) to describe the model of the scattering surface f.

Evaluating (4.2) at $y = h$, and noting $w(x,h) = u(x,h)$ and $w^\delta(x,h) = u^\delta(x,h)$, we have

$$w^\delta(x,h) = w_0(x,h) + \varepsilon w_1(x,h) + O(\varepsilon^2) + O(\delta). \tag{4.3}$$

Rearranging (4.3) yields

$$\varepsilon w_1(x,h) = \big(w^\delta(x,h) - w_0(x,h)\big) + O(\varepsilon^2) + O(\delta), \tag{4.4}$$

which is the basis of our inversion formula. Here the two parameters ε and δ indicate the ill-posed nature of the inverse problem; the larger the two parameters ε and δ are, the more severe the ill-posedness of the inverse problem is. Neglecting the asymptotic terms of ε^2 and δ in (4.4) yields

$$\varepsilon w_1(x,h) = w^\delta(x,h) - w_0(x,h), \tag{4.5}$$

which actually linearizes the inverse problem and may lead to an explicit inversion formula for the linearized inverse problem.

Based on (4.5), we next shall derive the analytical solution for the leading term w_0, deduce an equation relating w_1 and the scattering surface function f, and obtain an explicit inversion formula.

Recalling (3.9), (3.11), and (3.7), we have

$$\phi_0 = 0, \quad \psi_0 = \rho = -2\mathrm{i}\beta e^{\mathrm{i}(\alpha x - \beta h)}, \quad v_0 = 0.$$

which gives after taking the Fourier transform that

$$\hat{\phi}_0 = 0, \quad \hat{\psi}_0 = -2(2\pi)^{1/2}\mathrm{i}\beta\delta(\xi - \alpha)e^{-\mathrm{i}\beta h}, \quad \hat{v}_0 = 0.$$

It follows from the solution representation (3.15) in Theorem 3.1 that we have

$$\hat{w}_0(\xi, y) = -K_2(\xi, y)\hat{\psi}_0.$$

Taking the inverse Fourier transform with respect to x on both sides of the above equation yields

$$\begin{aligned} w_0(x,y) &= 2\mathrm{i}\beta e^{-\mathrm{i}\beta h}\int_{\mathbb{R}} K_2(\xi,y)\delta(\xi-\alpha)e^{\mathrm{i}\xi x}d\xi \\ &= 2\mathrm{i}\beta e^{-\mathrm{i}\beta h}K_2(\alpha,y)e^{\mathrm{i}\alpha x}. \end{aligned}$$

Noting the definition of K_2 and $\eta(\alpha)=\beta$, we have

$$K_2(\alpha,y)=\frac{e^{\mathrm{i}\beta(h-y)}}{2\beta(\mathrm{i}\beta-\nu)}[(\beta+\mathrm{i}\nu)+(\beta-\mathrm{i}\nu)e^{2\mathrm{i}\beta y}],$$

which gives the expression of the leading term for the asymptotic expansions

$$w_0(x,y)=\left[e^{-\mathrm{i}\beta y}+\left(\frac{\beta-\mathrm{i}\nu}{\beta+\mathrm{i}\nu}\right)e^{\mathrm{i}\beta y}\right]e^{\mathrm{i}\alpha x}=e^{\mathrm{i}(\alpha x-\beta y)}+\left(\frac{\beta-\mathrm{i}\nu}{\beta+\mathrm{i}\nu}\right)e^{\mathrm{i}(\alpha x+\beta y)}. \tag{4.6}$$

Denote $u^{\mathrm{ref}}(x,y)=((\beta-\mathrm{i}\nu)/(\beta+\mathrm{i}\nu))e^{\mathrm{i}(\alpha x+\beta y)}$. Clearly, u^{ref} represents an outgoing reflected plane wave. The leading term w_0 is just consisted of the incident field and the reflected field, i.e., $w_0=u^{\mathrm{inc}}+u^{\mathrm{ref}}$. It can be easily verified that w_0 satisfies the impedance condition on the flat plane $y=0$, i.e., $\partial_y w_0(x,0)-\nu w_0(x,0)=0$.

REMARK 4.1. *Physically, the leading term w_0 arises from the interaction of the incident field u^{inc} and the impedance plane surface. Mathematically, it satisfies the Helmholtz equation*

$$\frac{\partial^2 w_0}{\partial x^2}+\frac{\partial^2 w_0}{\partial y^2}+\kappa^2 w_0=0 \quad \text{in } D,$$

with the impedance boundary condition

$$\partial_y w_0-\nu w_0=0 \quad \text{on } y=0,$$

and the outgoing wave condition or the transparent boundary condition

$$\partial_y w_0=Tw_0+\rho \quad \text{on } y=h.$$

It can be verified that the solution w_0 consists of the incident field u^{inc} and the reflected field u^{ref}.

Next we derive the expression of w_1 in terms of the scattering surface function g. It follows from the expressions of (3.9) and (4.6) that we obtain

$$\begin{aligned} \phi_1(x) &= g'\partial_x w_0(x,0)-\nu\left(\frac{g}{h}\right)w_0(x,0) \\ &= 2\mathrm{i}\alpha\beta(\beta+\mathrm{i}\nu)^{-1}g'e^{\mathrm{i}\alpha x}-2\nu\beta(\beta+\mathrm{i}\nu)^{-1}h^{-1}ge^{\mathrm{i}\alpha x} \end{aligned}$$

Taking the Fourier transform of ϕ_1, we get

$$\hat{\phi}_1(\xi)=-2\beta(\beta+\mathrm{i}\nu)^{-1}(\alpha\xi+\nu h^{-1})\hat{g}(\xi-\alpha). \tag{4.7}$$

Recalling (3.11), (3.10), and (4.6), we have

$$\begin{aligned} \psi_1(x) &= -\left(\frac{g}{h}\right)(Tw_0+\rho)=-\left(\frac{g}{h}\right)\partial_y w_0 \\ &= \mathrm{i}\beta h^{-1}\left[e^{-\mathrm{i}\beta h}-\left(\frac{\beta-\mathrm{i}\nu}{\beta+\mathrm{i}\nu}\right)e^{\mathrm{i}\beta h}\right]g(x)e^{\mathrm{i}\alpha x}. \end{aligned}$$

Taking the Fourier transform of ψ_1 gives

$$\hat{\psi}_1(\xi) = \mathrm{i}\beta h^{-1}\left[e^{-\mathrm{i}\beta h} - \left(\frac{\beta-\mathrm{i}\nu}{\beta+\mathrm{i}\nu}\right)e^{\mathrm{i}\beta h}\right]\hat{g}(\xi-\alpha). \tag{4.8}$$

It follows from (3.7) that we have

$$v_1(x,y) = \frac{2g}{h}\frac{\partial^2 w_0}{\partial x^2} + \frac{2g'(h-y)}{h}\frac{\partial^2 w_0}{\partial x\partial y} + \frac{g''(h-y)}{h}\frac{\partial w_0}{\partial y} + \frac{2\kappa^2 g}{h}w_0.$$

Substituting the expression of w_0 in (4.6) into the right hand side of the above equation yields

$$\begin{aligned} v_1(x,y) = \frac{2(\kappa^2-\alpha^2)}{h}&\left[e^{-\mathrm{i}\beta y} + \left(\frac{\beta-\mathrm{i}\nu}{\beta+\mathrm{i}\nu}\right)e^{\mathrm{i}\beta y}\right]g(x)e^{\mathrm{i}\alpha x} + \frac{\beta(h-y)}{h} \\ &\times\left[e^{-\mathrm{i}\beta y} - \left(\frac{\beta-\mathrm{i}\nu}{\beta+\mathrm{i}\nu}\right)e^{\mathrm{i}\beta y}\right][2\alpha g'(x) - \mathrm{i}g''(x)]e^{\mathrm{i}\alpha x}. \end{aligned}$$

Taking the Fourier transform of v_1 with respect to x yields

$$\begin{aligned} \hat{v}_1(\xi,y) = \frac{2(\kappa^2-\alpha^2)}{h}&\left[e^{-\mathrm{i}\beta y} + \left(\frac{\beta-\mathrm{i}\nu}{\beta+\mathrm{i}\nu}\right)e^{\mathrm{i}\beta y}\right]\hat{g}(\xi-\alpha) + \frac{\mathrm{i}\beta(h-y)}{h} \\ &\times\left[e^{-\mathrm{i}\beta y} - \left(\frac{\beta-\mathrm{i}\nu}{\beta+\mathrm{i}\nu}\right)e^{\mathrm{i}\beta y}\right](2\xi\alpha+\xi^2)\hat{g}(\xi-\alpha). \end{aligned} \tag{4.9}$$

To simplify the tedious calculations, from now on, we consider the special case of a normal incidence for the incident field, i.e.,

$$\theta = 0,\ \alpha = 0,\ \beta = \kappa.$$

Otherwise, there is a phase shift of the reconstruction for other directions of incidence due to $\alpha \neq 0$. Under the normal incidence, (4.7), (4.8) and (4.9) can be reduced to

$$\hat{\phi}_1 = -2\nu\kappa(\kappa+\mathrm{i}\nu)^{-1}h^{-1}\,\hat{g}(\xi), \quad \hat{\psi}_1 = \mathrm{i}\kappa h^{-1}\left[e^{-\mathrm{i}\kappa h} - \left(\frac{\kappa-\mathrm{i}\nu}{\kappa+\mathrm{i}\nu}\right)e^{\mathrm{i}\kappa h}\right]\hat{g}(\xi),$$

and

$$\begin{aligned} \hat{v}_1(\xi,y) = \frac{2\kappa^2}{h}&\left[e^{-\mathrm{i}\kappa y} + \left(\frac{\kappa-\mathrm{i}\nu}{\kappa+\mathrm{i}\nu}\right)e^{\mathrm{i}\kappa y}\right]\hat{g}(\xi) + \frac{\mathrm{i}\kappa(h-y)\xi^2}{h} \\ &\times\left[e^{-\mathrm{i}\kappa y} - \left(\frac{\kappa-\mathrm{i}\nu}{\kappa+\mathrm{i}\nu}\right)e^{\mathrm{i}\kappa y}\right]\hat{g}(\xi). \end{aligned}$$

It follows from the explicit solution representation (3.15) in Theorem 3.1 that we have

$$\hat{w}_1(\xi,y) = K_1(\xi,y)\hat{\phi}_1(\xi) - K_2(\xi,y)\hat{\psi}_1(\xi) + \int_0^h K_3(\xi,y,z)\hat{v}_1(\xi,z)dz. \tag{4.10}$$

Since the data of the field is recorded at Γ, we evaluate (4.10) at $y = h$ and obtain

$$\hat{w}_1(\xi,h) = K_1(\xi,h)\hat{\phi}_1(\xi) - K_2(\xi,h)\hat{\psi}_1(\xi) + \int_0^h K_3(\xi,h,z)\hat{v}_1(\xi,z)dz, \tag{4.11}$$

where

$$K_1(\xi,h)=\frac{e^{\mathrm{i}\eta h}}{\mathrm{i}\eta-\nu},\quad K_2(\xi,h)=\frac{e^{\mathrm{i}\eta h}}{2\eta(\mathrm{i}\eta-\nu)}\Big[(\eta+\mathrm{i}\nu)e^{-\mathrm{i}\eta h}+(\eta-\mathrm{i}\nu)e^{\mathrm{i}\eta h}\Big]$$

and

$$K_3(\xi,h,z)=\frac{e^{\mathrm{i}\eta h}}{2\eta(\mathrm{i}\eta-\nu)}\Big[(\eta+\mathrm{i}\nu)e^{-\mathrm{i}\eta z}+(\eta-\mathrm{i}\nu)e^{\mathrm{i}\eta z}\Big].$$

Define

$$M_1=K_1(\xi,h)\hat{\phi}_1(\xi),\ M_2=K_2(\xi,h)\hat{\psi}_1(\xi),\ M_3=\int_0^h K_3(\xi,h,z)\hat{v}_1(\xi,z)dz. \tag{4.12}$$

Using the definitions of K_1 and $\hat{\phi}_1$, we have

$$M_1=-\frac{2\nu\kappa e^{\mathrm{i}\eta h}}{h(\mathrm{i}\eta-\nu)(\kappa+\mathrm{i}\nu)}\,\hat{g}(\xi). \tag{4.13}$$

Using the definitions of K_2 and $\hat{\psi}_1$, we get

$$\begin{aligned}M_2&=\frac{\mathrm{i}\kappa e^{\mathrm{i}\eta h}}{2h\eta(\mathrm{i}\eta-\nu)(\kappa+\mathrm{i}\nu)}\Big[(\eta+\mathrm{i}\nu)e^{-\mathrm{i}\eta h}+(\eta-\mathrm{i}\nu)e^{\mathrm{i}\eta h}\Big]\times\Big[(\kappa+\mathrm{i}\nu)e^{-\mathrm{i}\kappa h}-(\kappa-\mathrm{i}\nu)e^{\mathrm{i}\kappa h}\Big]\hat{g}(\xi)\\&=\frac{\mathrm{i}\kappa e^{\mathrm{i}\eta h}}{2h\eta(\mathrm{i}\eta-\nu)(\kappa+\mathrm{i}\nu)}\Big[(\eta+\mathrm{i}\nu)(\kappa+\mathrm{i}\nu)e^{-\mathrm{i}(\eta+\kappa)h}-(\eta+\mathrm{i}\nu)(\kappa-\mathrm{i}\nu)e^{-\mathrm{i}(\eta-\kappa)h}\\&\qquad+(\eta-\mathrm{i}\nu)(\kappa+\mathrm{i}\nu)e^{\mathrm{i}(\eta-\kappa)h}-(\eta-\mathrm{i}\nu)(\kappa-\mathrm{i}\nu)e^{\mathrm{i}(\eta+\kappa)h}\Big]\hat{g}(\xi).\end{aligned} \tag{4.14}$$

Using the definitions of K_3 and $\hat{v}_1$, we obtain

$$M_3=N_1+N_2, \tag{4.15}$$

where

$$\begin{aligned}N_1=\frac{\kappa^2e^{\mathrm{i}\eta h}}{h\eta(\mathrm{i}\eta-\nu)(\kappa+\mathrm{i}\nu)}\int_0^h&\Big[(\eta+\mathrm{i}\nu)e^{-\mathrm{i}\eta z}+(\eta-\mathrm{i}\nu)e^{\mathrm{i}\eta z}\Big]\\&\times\Big[(\kappa+\mathrm{i}\nu)e^{-\mathrm{i}\kappa z}+(\kappa-\mathrm{i}\nu)e^{\mathrm{i}\kappa z}\Big]\hat{g}(\xi)\,dz,\end{aligned}$$

and

$$\begin{aligned}N_2=\frac{\mathrm{i}\kappa\xi^2e^{\mathrm{i}\eta h}}{2h\eta(\mathrm{i}\eta-\nu)(\kappa+\mathrm{i}\nu)}\int_0^h&\Big[(\eta+\mathrm{i}\nu)e^{-\mathrm{i}\eta z}+(\eta-\mathrm{i}\nu)e^{\mathrm{i}\eta z}\Big](h-z)\\&\times\Big[(\kappa+\mathrm{i}\nu)e^{-\mathrm{i}\kappa z}-(\kappa-\mathrm{i}\nu)e^{\mathrm{i}\kappa z}\Big]\hat{g}(\xi)\,dz.\end{aligned}$$

Following from direct integrations yields

$$\begin{aligned}N_1=\frac{\mathrm{i}\kappa^2e^{\mathrm{i}\eta h}}{h\eta(\mathrm{i}\eta-\nu)(\kappa+\mathrm{i}\nu)}\Big[&\frac{(\eta-\mathrm{i}\nu)(\kappa-\mathrm{i}\nu)}{(\eta+\kappa)}\Big(1-e^{\mathrm{i}(\eta+\kappa)h}\Big)+\frac{(\eta-\mathrm{i}\nu)(\kappa+\mathrm{i}\nu)}{(\eta-\kappa)}\Big(1-e^{\mathrm{i}(\eta-\kappa)h}\Big)\\&-\frac{(\eta+\mathrm{i}\nu)(\kappa+\mathrm{i}\nu)}{(\eta+\kappa)}\Big(1-e^{-\mathrm{i}(\eta+\kappa)h}\Big)-\frac{(\eta+\mathrm{i}\nu)(\kappa-\mathrm{i}\nu)}{(\eta-\kappa)}\Big(1-e^{-\mathrm{i}(\eta-\kappa)h}\Big)\Big]\hat{g}(\xi).\end{aligned}$$

Using integration by parts and the identity $\eta^2+\xi^2=\kappa^2$, we have from tedious but straightforward calculations that

$$N_2=\frac{2\kappa(\kappa^2+\nu^2)e^{\mathrm{i}\eta h}}{(\mathrm{i}\eta-\nu)(\kappa+\mathrm{i}\nu)}\,\hat{g}(\xi)+\frac{\mathrm{i}\kappa e^{\mathrm{i}\eta h}}{2h\eta(\mathrm{i}\eta-\nu)(\kappa+\mathrm{i}\nu)}\bigg[\frac{(\eta-\mathrm{i}\nu)(\kappa-\mathrm{i}\nu)(\eta-\kappa)}{(\eta+\kappa)}\left(1-e^{\mathrm{i}(\eta+\kappa)h}\right)$$
$$-\frac{(\eta-\mathrm{i}\nu)(\kappa+\mathrm{i}\nu)(\eta+\kappa)}{(\eta-\kappa)}\left(1-e^{\mathrm{i}(\eta-\kappa)h}\right)-\frac{(\eta+\mathrm{i}\nu)(\kappa+\mathrm{i}\nu)(\eta-\kappa)}{(\eta+\kappa)}\left(1-e^{-\mathrm{i}(\eta+\kappa)h}\right)$$
$$+\frac{(\eta+\mathrm{i}\nu)(\kappa-\mathrm{i}\nu)(\eta+\kappa)}{(\eta-\kappa)}\left(1-e^{-\mathrm{i}(\eta-\kappa)h}\right)\bigg]\,\hat{g}(\xi).$$

Adding N_1 and N_2, and noting (4.15) gives

$$M_3=\frac{2\kappa(\kappa^2+\nu^2)e^{\mathrm{i}\eta h}}{(\mathrm{i}\eta-\nu)(\kappa+\mathrm{i}\nu)}\,\hat{g}(\xi)+\frac{\mathrm{i}\kappa e^{\mathrm{i}\eta h}}{2h\eta(\mathrm{i}\eta-\nu)(\kappa+\mathrm{i}\nu)}\bigg[(\eta-\mathrm{i}\nu)(\kappa-\mathrm{i}\nu)\left(1-e^{\mathrm{i}(\eta+\kappa)h}\right)$$
$$-(\eta-\mathrm{i}\nu)(\kappa+\mathrm{i}\nu)\left(1-e^{\mathrm{i}(\eta-\kappa)h}\right)-(\eta+\mathrm{i}\nu)(\kappa+\mathrm{i}\nu)\left(1-e^{-\mathrm{i}(\eta+\kappa)h}\right)$$
$$+(\eta+\mathrm{i}\nu)(\kappa-\mathrm{i}\nu)\left(1-e^{-\mathrm{i}(\eta-\kappa)h}\right)\bigg]\,\hat{g}(\xi). \tag{4.16}$$

Subtracting 4.14 from (4.16) leads to

$$M_3-M_2=\frac{2\kappa(\kappa^2+\nu^2)e^{\mathrm{i}\eta h}}{(\mathrm{i}\eta-\nu)(\kappa+\mathrm{i}\nu)}\,\hat{g}(\xi)+\frac{2\nu\kappa e^{\mathrm{i}\eta h}}{h(\mathrm{i}\eta-\nu)(\kappa+\mathrm{i}\nu)}\,\hat{g}(\xi). \tag{4.17}$$

Finally, adding (4.13) and (4.17) and noting (4.11) and (4.12), we obtain an elegant equation relating w_1 and g:

$$\hat{w}_1(\xi,h)=M_3-M_2+M_1=\frac{2\kappa(\kappa^2+\nu^2)e^{\mathrm{i}\eta h}}{(\mathrm{i}\eta-\nu)(\kappa+\mathrm{i}\nu)}\,\hat{g}(\xi)=\frac{2\kappa(\kappa-\mathrm{i}\nu)e^{\mathrm{i}\eta h}}{(\mathrm{i}\eta-\nu)}\,\hat{g}(\xi). \tag{4.18}$$

Noting $\hat{f}=\varepsilon\hat{g}$ and combining (4.5) and (4.18), we deduce an explicit inversion formula to reconstruct the scattering surface function:

$$\hat{f}_{\varepsilon,\delta}(\xi)=\frac{(\mathrm{i}\eta-\nu)}{2\kappa(\kappa-\mathrm{i}\nu)}\left(\hat{w}^{\delta}(\xi,h)-\hat{w}_0(\xi,h)\right)e^{-\mathrm{i}\eta h}. \tag{4.19}$$

Here the subscript ε and δ indicate the dependence of the reconstruction on these two parameters.

Remark 4.2. *The factor on the right hand side of* (4.19)*, $e^{-\mathrm{i}\eta h}$, exactly reflects the ill-posedness of the inverse problem, i.e,. the measurement noise will be exponentially amplified for high frequency modes with $|\xi|>\kappa$.*

Remark 4.3. *The inversion formula* (4.19) *includes the cases for the sound hard and the sound soft boundary conditions. For the sound hard boundary condition, i.e., $\lambda=0$, the inversion formula* (4.19) *reduces to*

$$\hat{f}_{\varepsilon,\delta}(\xi)=\frac{\mathrm{i}\eta}{2\kappa^2}\left(\hat{w}^{\delta}(\xi,h)-\hat{w}_0(\xi,h)\right)e^{-\mathrm{i}\eta h}; \tag{4.20}$$

for the sound soft boundary condition, i.e., $\lambda=\infty$, the inversion formula (4.19) *reduces to*

$$\hat{f}_{\varepsilon,\delta}(\xi)=-\frac{\mathrm{i}}{2\kappa}\left(\hat{w}^{\delta}(\xi,h)-\hat{w}_0(\xi,h)\right)e^{-\mathrm{i}\eta h}. \tag{4.21}$$

In numerical experiments, we shall focus on the case of the sound soft boundary condition to illustrate the performance of the proposed method.

REMARK 4.4. *The inversion formula* (4.19) *makes use of both propagation wave modes and evanescent wave modes. More explicitly, we have*

$$\hat{f}_{\varepsilon,\delta}(\xi) = \begin{cases} \dfrac{[\mathrm{i}(\kappa^2-\xi^2)^{1/2}-\nu]}{2\kappa(\kappa-\mathrm{i}\nu)}\left(\hat{w}^\delta(\xi,h)-\hat{w}_0(\xi,h)\right)e^{-\mathrm{i}(\kappa^2-\xi^2)^{1/2}h} & \text{for} \quad |\xi|<\kappa, \\ \dfrac{[(\xi^2-\kappa^2)^{1/2}+\nu]}{2\kappa(\kappa-\mathrm{i}\nu)}\left(\hat{w}_0(\xi,h)-\hat{w}^\delta(\xi,h)\right)e^{(\xi^2-\kappa^2)^{1/2}h} & \text{for} \quad |\xi|>\kappa. \end{cases}$$

Clearly, the low frequency modes of the scattering surface function f come from the propagation waves; while the evanescent waves contribute to the high frequency modes of the scattering surface function f, which do not obey the Rayleigh criterion and display super resolution.

As shown in Remark 4.4, it is well-posed to reconstruct the scattering surface function with the Fourier modes less than the wavenumber κ in the sense that small variations in the measured data will not lead to large errors in the reconstruction. Thus, no regularization is needed for the inversion formula (4.19) when $|\xi|<\kappa$. However, it is severely ill-posed to reconstruct the scattering surface function with the Fourier modes greater than the wavenumber κ, which is unlike the reconstruction for the low frequency propagation modes. Small variations in the measured data will be exponentially enlarged and lead to huge errors in the reconstruction. Thus, regularization must be considered to suppress the exponential growth of the reconstruction errors for the inversion formula (4.19) when $|\xi|>\kappa$.

There are two aspects to remedy the ill-posedness of the inversion formula (4.19) and thus to obtain a stable and super-resolved reconstruction. One aspect is to make h as small as possible, i.e., measure the data at the height which is as close as possible to scattering surface. This is exactly the idea of near-field optics: by bringing a scanning tip into the near-field (subwavelength) of the sample, the high frequency evanescent field can be detected, and thus images with subwavelength resolution may be obtained. Besides, another aspect is to adopt a commonly used regularization technique such as spectral cut-off or Tikhonov regularization [22]. We do not discuss here the relative advantages or disadvantages of different regularization methods. Following [8], we consider only the cut-off regularization. For a fixed distance h, the cutoff frequency ω depends on the noise level δ and the surface deformation parameter ε. Define the signal-to-noise ratio (SNR) by

$$\mathrm{SNR} = \min\{\varepsilon^{-2},\ \delta^{-1}\},$$

which measures the noise level and the surface deformation parameter. We choose the cut-off frequency in such a way that

$$e^{(\omega^2-\kappa^2)^{1/2}h} = \mathrm{SNR},$$

which implies that the spatial frequency will be cutoff for those below the noise level and the surface deformation parameter. More explicitly, we have

$$\frac{\omega}{\kappa} = \left[1+\left(\frac{\log \mathrm{SNR}}{\kappa h}\right)^2\right]^{1/2}, \tag{4.22}$$

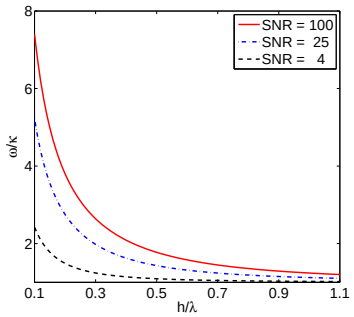

FIG. 4.1. *The ratio between the cut-off frequency and the background wavenumber ω/κ is plotted against the measurement distance h/λ for different signal-to-noise ratio (SNR).*

which implies $\omega > \kappa$ as long as SNR > 0 and super resolution may be achieved.

In Figure 4.1, we plot the ratio between the cut-off frequency ω and the background wavenumber κ, i.e., ω/κ, for various distance h with SNR=100, 25, 4. As can be seen, the cut-off frequency $\omega >> \kappa$ when $h << \lambda$ for fixed SNR, i.e., the bandwidth of the spatial frequency in the near-field is much larger than that in the far-field; the smaller the SNR is, the larger ω/κ is, i.e., better resolution can be achieved for lower noise level and smaller surface deformation parameter.

Taking into account the frequency cut-off, we have a regularized inversion formulation for (4.19):

$$\hat{f}_{\varepsilon,\delta}(\xi) = \frac{(\mathrm{i}\eta - \nu)}{2\kappa(\kappa - \mathrm{i}\nu)} \left(\hat{w}^{\delta}(\xi, h) - \hat{w}_0(\xi, h)\right) e^{-\mathrm{i}\eta h}\, \chi_{[-\omega,\,\omega]}(\xi), \tag{4.23}$$

where the characteristic function

$$\chi_{[-\omega,\,\omega]}(\xi) = \begin{cases} 1 & \text{for} \quad |\xi| \le \omega, \\ 0 & \text{for} \quad |\xi| > \omega. \end{cases}$$

Define

$$\tilde{f}_0(\xi) = \frac{(\mathrm{i}\eta - \nu)}{2\kappa(\kappa - \mathrm{i}\nu)} \hat{w}_0(\xi, h) e^{-\mathrm{i}\eta h}\, \chi_{[-\omega,\,\omega]}(\xi) \tag{4.24}$$

and

$$\tilde{f}_1(\xi) = \frac{(\mathrm{i}\eta - \nu)}{2\kappa(\kappa - \mathrm{i}\nu)} \hat{w}^{\delta}(\xi, h) e^{-\mathrm{i}\eta h}\, \chi_{[-\omega,\,\omega]}(\xi). \tag{4.25}$$

It follows from the regularized inversion formulation (4.23) that we obtain the reconstructed scattering surface after taking the inverse Fourier transform:

$$\tilde{f}(x) = (2\pi)^{-1/2} \int_{\mathbb{R}} [\tilde{f}_1(\xi) - \tilde{f}_0(\xi)] e^{\mathrm{i}\xi x} d\xi. \tag{4.26}$$

Clearly, the reconstructed scattering surface function $\tilde{f}$ depends on the cut-off frequency ω, which depends on the scattering surface deformation parameter ε and the data noise level parameter δ.

For the normal incidence, the leading term w_0 in (4.6) becomes

$$w_0(x,h) = e^{-\mathrm{i}\kappa h} + \left(\frac{\kappa+\nu}{\kappa-\nu}\right) e^{\mathrm{i}\kappa h},$$

which is after taking the Fourier transform with respect to x

$$\hat{w}_0(\xi,y) = (2\pi)^{1/2}\left[e^{-\mathrm{i}\kappa h} + \left(\frac{\kappa+\nu}{\kappa-\nu}\right) e^{\mathrm{i}\kappa h}\right]\delta(\xi).$$

Simple calculation yields

$$(2\pi)^{-1/2}\int_{\mathbb{R}} \tilde{f}_0(\xi)e^{\mathrm{i}\xi x}d\xi = \frac{\mathrm{i}(\kappa+\mathrm{i}\nu)}{2\kappa(\kappa-\mathrm{i}\nu)}\left[e^{-2\mathrm{i}\kappa h} + \left(\frac{\kappa+\nu}{\kappa-\nu}\right)\right].$$

The regularized inversion formula (4.26) can be finally written as

$$\tilde{f}(x) = (2\pi)^{-1/2}\int_{\mathbb{R}} \tilde{f}_1(\xi)e^{\mathrm{i}\xi x}d\xi - \frac{\mathrm{i}(\kappa+\mathrm{i}\nu)}{2\kappa(\kappa-\mathrm{i}\nu)}\left[e^{-2\mathrm{i}\kappa h} + \left(\frac{\kappa+\nu}{\kappa-\nu}\right)\right]. \tag{4.27}$$

REMARK 4.5. *For the sound hard boundary condition, i.e., $\nu = 0$, the regularized inversion formula* (4.27) *is reduced to*

$$\tilde{f}(x) = (2\pi)^{-1/2}\int_{\mathbb{R}} \tilde{f}_1(\xi)e^{\mathrm{i}\xi x}d\xi - \frac{\mathrm{i}e^{-\mathrm{i}\kappa h}}{\kappa}\cos(\kappa h), \tag{4.28}$$

where

$$\tilde{f}_1(\xi) = \frac{\mathrm{i}\eta}{2\kappa^2}\hat{w}^\delta(\xi,h)e^{-\mathrm{i}\eta h}\,\chi_{[-\omega,\,\omega]}(\xi);$$

for the sound soft boundary condition, i.e., $\nu = \infty$, the regularized inversion formula (4.27) *is reduced to*

$$\tilde{f}(x) = \frac{e^{-\mathrm{i}\kappa h}}{\kappa}\sin(\kappa h) - (2\pi)^{-1/2}\int_{\mathbb{R}} \tilde{f}_1(\xi)e^{\mathrm{i}\xi x}d\xi, \tag{4.29}$$

where

$$\tilde{f}_1(\xi) = \frac{\mathrm{i}}{2\kappa}\hat{w}^\delta(\xi,h)e^{-\mathrm{i}\eta h}\,\chi_{[-\omega,\,\omega]}(\xi).$$

As shown in (4.25) and (4.27), one Fourier transform and one inverse Fourier transform are needed to reconstruct the scattering surface function. These transforms are realized by the fast Fourier transform (FFT) in our numerical experiments.

5. Numerical experiments. In this section, we discuss the algorithmic implementation for the direct and inverse surface scattering problems, present two numerical examples to illustrate the effectiveness of the proposed method, and examine the dependence of resolution on parameters measurement distance h, surface deformation parameter ε, and the noise level δ. Since the results are similar for the sound soft, sound hard, and impedance boundary conditions, we shall only present the examples for the sound soft boundary condition. Two types of surfaces were considered: locally perturbed surface with a compact support in Example 1 and an oscillatory periodic surface in Example 2, as seen in Figure 5.1.

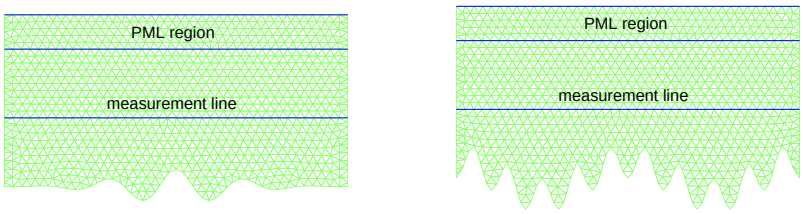

FIG. 5.1. *Scattering surfaces (even functions) and meshes of computational domains. Periodic boundary condition is imposed in the x direction and the perfectly matched layer technique is adopted in the y direction. (left) Locally perturbed surface with a compact support for Example 1; (right) Highly oscillatory periodic surface for Example 2.*

In practice, the open domain needs to be truncated into a bounded domain in order to solve the direct problem and obtain the synthetic scattering data. Suitable boundary conditions have to be imposed on the boundary of the bounded domain so that no artificial wave reflection occurs to ruin the wave field inside the domain. In Section 2, a transparent boundary condition is introduced in the y direction. However, this non-reflecting boundary condition is nonlocal and involves the issue of the Fourier transform in the whole $\mathbb{R}$. Besides, an appropriate boundary condition needs to be considered in the x direction. Since the focus is on the inverse problem in this work, we consider special examples: the scattering surfaces are even functions. Due to the symmetry of the problem, normal incidence and even scattering surfaces, the solutions to the direct problem are also symmetric to the y axis and thus the periodic boundary condition can be used in the x direction. In the y direction, we adopted a convenient perfectly matched layer (PML) technique to truncate the open domain [15]. Due to the periodicity of the solutions, we modified a simple mesh generator in MATLAB by Persson and Strang [35] to maintain the periodicity of the meshes in the x direction. The scattering data were obtained by the numerical solution of the direct scattering problem, which was implemented by using the finite element method.

In the following two examples, the incident wave was taken as a single plane wave with normal incidence, i.e., $u^{\text{inc}}(x, y) = e^{-\mathrm{i}\kappa y}$. The wavenumber was $\kappa = 2\pi$ which corresponds to the wavelength $\lambda = 1$. In all the figures, the plots were rescaled with respect to the wavelength λ. Due to the unstructured triangular meshes, the wave field data $u(x, h)$ was not equally spaced with respect to x. We constructed a curve $u(x, h)$ by using the natural cubic spline interpolation formula based on the computed discrete data $u(x, h)$. The curve $u(x, h)$ was evaluated at equally spaced points $x_j, j = 0, 1, \ldots, 512$, in the interval $[-0.5, 0.5]$, and used as our synthetic scattering data.

Example 1: This example illustrates the results for a locally perturbed plane surface, as seen in the left of Figure 5.1. The exact scattering surface is given by $f(x) = \varepsilon g(x)$, where

$$g(x) = \cos(10\pi x)e^{-20x^2}.$$

The computational domain for the direct problem is $[-0.5,\ 0.5] \times [f,\ 1.0]$ with the

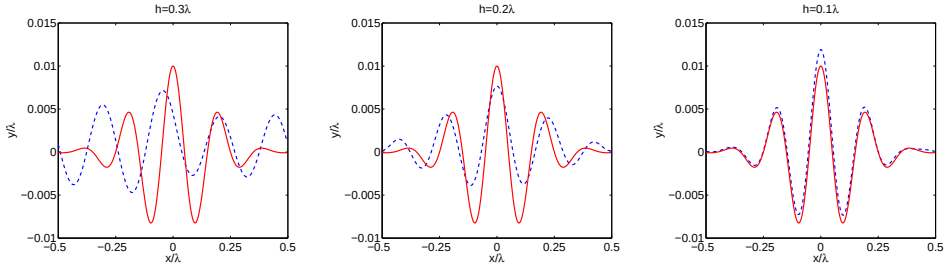

FIG. 5.2. *Example 1: locally perturbed surface; exact surface (solid line) and reconstructed surface (dashed line) using the scattering data measured at distance* $h = 0.3\lambda, 0.2\lambda, 0.1\lambda$.

PML region $[-0.5,\ 0.5] \times [0.8,\ 1.0]$. We examine the effects of h, δ, and ε on the reconstructions.

First consider the measurement distance h. The surface deformation parameter was fixed as $\varepsilon = 0.01$. No additional noise was added to the data except for the error from the linearization by dropping the high order terms in the asymptotic expansion. Figure 5.2 shows the reconstructed surface (dashed line) against the exact surface (solid line) by using the scattering data measured at different distances $h = 0.3\lambda, 0.2\lambda, 0.1\lambda$. It is clear that smaller measurement distance gives better reconstruction result. The fine features of the scattering surface is completely recovered and the subwavelength resolution is obviously achieved especially when using $h = 0.1\lambda$. This is attributed to the fact that larger cut-off frequency ω may be used in the inversion formula when the measurement distance h is smaller for fixed SNR, i.e., fixed ε and δ.

Next consider the noise level parameter δ. To test the stability of the method, some relative random noise was added to the scattering data, i.e., the scattering data took

$$u^\delta(x, h) = u(x, h)(1 + \delta\,\mathrm{rand}),$$

where rand stands for uniformly distributed random numbers in $[-1,\ 1]$. The surface deformation parameter and the measurement distance were fixed as $\varepsilon = 0.01$ and $h = 0.04\lambda$, respectively. Figure 5.3 plots the reconstructed surface (dashed line) against the exact surface (solid line) by using the scattering data with different noise level $\delta = 0.01, 0.03, 0.05$. It can be seen that smaller noise level yields better reconstruction result. As expected from the relation between the cut-off frequency and the SNR in (4.22), larger noise level parameter δ means smaller SNR and thus smaller cut-off frequency ω in order to get a stable reconstruction.

Finally consider the surface deformation parameter ε. The measurement distance $h = 0.08\lambda$ and again no additional noise was added to the data. Figure 5.4 shows the reconstructed surface (dashed line) against the exact surface (solid line) by using the scattering data with different surface deformation parameter $\varepsilon = 0.01, 0.02, 0.04$. Clearly, smaller ε gives better reconstruction. All the fine features are recovered especially when using $\varepsilon = 0.01$. Although some amplitude information are not completely correct, all the phase information are still correctly reconstructed even for large ε. Following the asymptotic expansion (4.2), the linearization procedure (4.5) gives more accurate approximation to the original nonlinear inverse problem if the surface deformation parameter ε is smaller. For fixed ε and h, smaller δ means larger

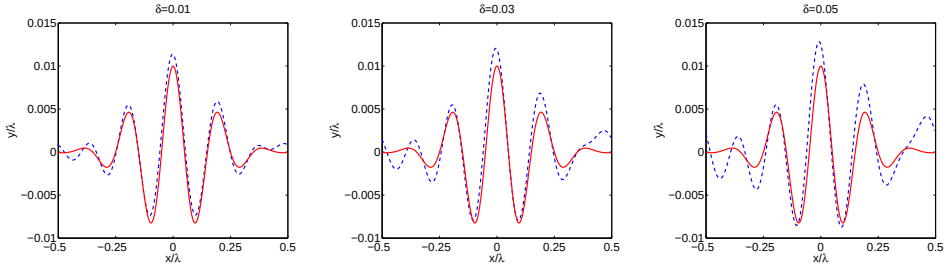

FIG. 5.3. *Example 1: locally perturbed surface; exact surface (solid line) and reconstructed surface (dashed line) using the scattering data with noise level* $\delta = 0.01, \delta = 0.03, \delta = 0.05$.

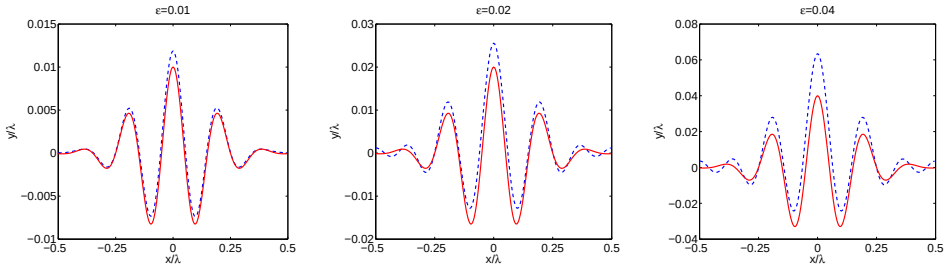

FIG. 5.4. *Example 1: locally perturbed surface; exact surface (solid line) and reconstructed surface (dashed line) with surface deformation parameter* $\varepsilon = 0.01, \varepsilon = 0.02, \varepsilon = 0.04$.

SNR and thus larger cut-off frequency ω, which contributes to a better and sharper reconstruction.

Based on the above observation, it can be concluded that smaller measurement distance (as small as possible) is preferred in order to obtain a stable reconstruction with a super resolved resolution, which confirms the principle of near-field optical imaging.

Example 2: This example uses a more oscillatory periodic scattering surface to illustrates the results for a non-locally perturbed plane surface, as seen in the right of 5.1. The exact scattering surface is described by the periodic function $f(x) = \varepsilon g(x)$ with $\varepsilon = 0.005$ and

$$g(x) = \cos(4\pi x) - \cos(20\pi x).$$

The computational domain is $[-0.5,\ 0.5] \times [f,\ 0.5]$ with the PML region $[-0.5,\ 0.5] \times [0.3,\ 0.5]$. For this example, we will not show the investigation of the reconstructions on all the parameters since the results and conclusions are the same as those for the first example. This scattering surface is much more oscillatory and has finer features than the first example does. It is expected to use larger cut-off frequency ω in order to completely resolve all the features and get a super resolved resolution for the construction, which requires smaller measurement distance h. Figure (5.5) shows the reconstructed surface (dashed line) against the exact surface (solid line) by using the scattering data with three pairs of different h and δ: (h, δ): $(h = 0.05\lambda,\ \delta = 0.01); (h = 0.04\lambda,\ \delta = 0.02); (h = 0.03\lambda,\ \delta = 0.05)$. Again, it can be seen that smaller surface deformation parameter h is needed in order to achieve equally good reconstruction for larger noise level parameter δ.

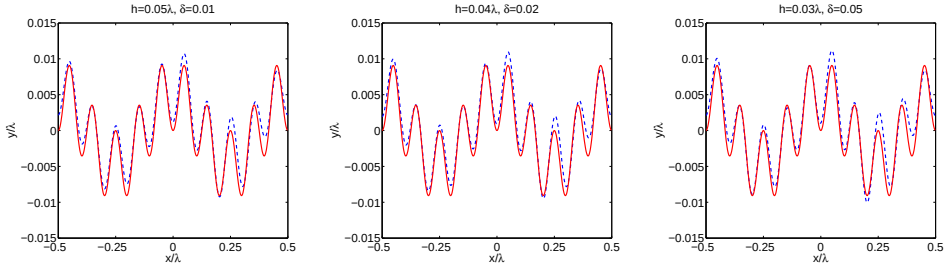

FIG. 5.5. *Example 2: highly oscillatory periodic scattering surface; exact surface (solid line) and reconstructed surface (dashed line) with three pairs of parameters* (h, δ)*:* $(h = 0.05\lambda,\ \delta = 0.01); (h = 0.04\lambda,\ \delta = 0.02); (h = 0.03\lambda,\ \delta = 0.05)$.

6. Concluding remarks. We presented a simple, stable, and effective method for solving an inverse surface scattering problem in near-field optical imaging. The scattering surface model was assumed to be a small and smooth deformation of a plane surface. Using transformed field expansion, we converted the scattering problem with a complex scattering surface into a successive sequence of a two-point boundary value problem in the frequency domain. We deduced an analytical solution for the direct scattering problem from the method of integration solution. By dropping the high order terms in the power series expansion, we linearized the nonlinear inverse problem and obtained an explicit and unified inversion formula for both the propagation and evanescent wave modes. The cut-off frequency was chosen from the SNR analysis which depends on the surface deformation parameter, noise level, and the measurement distance. The method works for sound soft, sound hard, and impedance scattering surfaces. The reconstruction method requires only a single illumination at a fixed frequency and is implemented efficiently by executing two FFTs, one is for the data processing and another is for the inversion. Two types of scattering surfaces were considered, a locally perturbed surface and an oscillatory periodic surface. The effects of the deformation parameter, noise level, and measurement distance were reported on the resolution of the reconstruction. The results show that super resolved resolution may be achieved for small measurement distance, which confirms the principle of near-field optical imaging.

We point out some future directions along the line of inverse surface scattering in near-field imaging. This paper considers the perfect electric conductor scattering surface. It is worthwhile to investigate the scattering surface for the transmission problem where the incident wave may penetrate the scattering surface. Similar inversion formulas are expected to be able to efficiently reconstruct the scattering surface for this problem. In this paper, the scattering surface is assumed to be a small deformation of a plane surface and the linearized inverse problem is a good approximation to the original nonlinear inverse problem. Results show that the accuracy of the reconstruction is deteriorated as the deformation parameter is increased. Thus the linear mode may not be sufficient and the nonlinear model needs to be considered for scattering surfaces with large deviation. Other interesting and challenging problems are to solve the inverse surface scattering using phaseless data and the model of Maxwell's equations for electromagnetic wave propagation. We hope to be able to address these issues and report the progress elsewhere in the future.

Acknowledgments. The authors thank the reviewers for their helpful comments to improve the manuscript.

Appendix A. Integration solution method.

In this section, the integrated solution method is briefly introduced to solve a two-point boundary value problem. We refer to Zhang [40] for the details of the integrated solutions of ordinary differential equation system and two-point boundary value problems.

Consider the two-point boundary value problem

$$\mathbf{u}'(y) + M(y)\mathbf{u}(y) = \mathbf{f}(y), \tag{A.1}$$

$$A_0\mathbf{u}(y)|_{y=0} = \mathbf{r}_0, \tag{A.2}$$

$$B_1\mathbf{u}(y)|_{y=h} = \mathbf{s}_1, \tag{A.3}$$

where $\mathbf{f}(y) \in \mathbb{C}^m$ are m-dimensional vector fields, $\mathbf{r}_0 \in \mathbb{C}^{m_1}$ and $\mathbf{s}_1 \in \mathbb{C}^{m_2}$ are given m_1- and m_2-dimensional vector fields, respectively, $M(y) \in \mathbb{C}^{m\times m}$ is an $m\times m$ matrix, and $A_0 \in \mathbb{C}^{m_1\times m}$ and $B_1 \in \mathbb{C}^{m_2\times m}$ are full rank matrices with $m_1 + m_2 = m$, i.e., $\mathrm{rank}A_0 = m_1$ and $\mathrm{rank}B_1 = m_2$.

Let $\Phi(y)$ be the fundamental matrix of the system

$$\Phi'(y) + M(y)\Phi(y) = \mathbf{0}, \tag{A.4}$$

$$\Phi(0) = I_m, \tag{A.5}$$

where I_m is the $m \times m$ identity matrix.

THEOREM A.1. *The two-point boundary value problem* (A.1)–(A.3) *has a unique solution if and only if*

$$\det\begin{bmatrix} A_0 \\ B_1\Phi(h) \end{bmatrix} \neq 0. \tag{A.6}$$

Let the pair of functions $\{A(y), \mathbf{r}(y)\}$ and $\{B(y), \mathbf{s}(y)\}$ be the integrated solutions of the problems (A.1)–(A.2) and (A.1)–(A.3), respectively, then there exist $D_0(A, y) \in \mathbb{C}^{m_1\times m_1}$ and $D_1(B, y) \in \mathbb{C}^{m_2\times m_2}$ such that

$$A' = AM + D_0A, \quad A(0) = A_0, \tag{A.7}$$

$$\mathbf{r}' = A\mathbf{f} + D_0\mathbf{r}, \quad \mathbf{r}(0) = \mathbf{r}_0, \tag{A.8}$$

and

$$B' = BM + D_1B, \quad B(h) = B_1, \tag{A.9}$$

$$\mathbf{s}' = B\mathbf{f} + D_1\mathbf{s}, \quad \mathbf{s}(h) = \mathbf{s}_1. \tag{A.10}$$

THEOREM A.2. *If the two-point boundary value problem* (A.1)–(A.3) *has a unique solution, then the matrix*

$$\begin{bmatrix} A(y) \\ B(y) \end{bmatrix} \in \mathbb{C}^{m\times m}$$

is nonsingular.

THEOREM A.3. *The two-point boundary value problem* (A.1)–(A.3) *is equivalent to the linear system*

$$\begin{bmatrix} A(y) \\ B(y) \end{bmatrix} \mathbf{u}(y) = \begin{bmatrix} \mathbf{r}(y) \\ \mathbf{s}(y) \end{bmatrix}. \tag{A.11}$$

Appendix B. A two-point boundary value problem.

In this section, we discuss the integration method for solving a two-point boundary value problem in details. Consider the second order boundary value problem

$$u'' + \eta^2 u = v, \quad 0 < y < h, \tag{B.1}$$

$$u' - \lambda u = \phi \quad \text{at } y = 0, \tag{B.2}$$

$$u' - \mathrm{i}\eta u = \psi \quad \text{at } y = h. \tag{B.3}$$

Let $u_1 = u$ and $u_2 = u'$. The second-order boundary value problem (B.1)–(B.3) can be equivalently formulated into a first-order two-point boundary value problem:

$$\mathbf{u}' + M\mathbf{u} = \mathbf{v}, \tag{B.4}$$

$$A_0\mathbf{u}(0) = \phi, \tag{B.5}$$

$$B_1\mathbf{u}(h) = \psi, \tag{B.6}$$

where

$$\mathbf{u} = \begin{bmatrix} u_1 \\ u_2 \end{bmatrix}, \quad \mathbf{v} = \begin{bmatrix} 0 \\ v \end{bmatrix}, \quad M = \begin{bmatrix} 0 & -1 \\ \eta^2 & 0 \end{bmatrix},$$

and

$$A_0 = [-\lambda \quad 1], \quad B_1 = [-\mathrm{i}\eta \quad 1].$$

LEMMA B.1. *Let $\lambda \neq \mathrm{i}\eta$. The two-point boundary value problem* (B.1)–(B.3) *has a unique solution given by*

$$u(y) = K_1(y)\phi - K_2(y)\psi + \int_0^h K_3(y,z)v(z)dz, \tag{B.7}$$

where

$$K_1(y) = \frac{e^{\mathrm{i}\eta y}}{\mathrm{i}\eta - \lambda}, \quad K_2(y) = \frac{e^{\mathrm{i}\eta(h-y)}}{\mathrm{i}\eta - \lambda}K(y), \quad K_3(y,z) = \begin{cases} \dfrac{e^{\mathrm{i}\eta(y-z)}}{\mathrm{i}\eta - \lambda}K(z), & z < y, \\ \dfrac{e^{\mathrm{i}\eta(z-y)}}{\mathrm{i}\eta - \lambda}K(y), & z > y. \end{cases}$$

Here

$$K(t) = \frac{(\eta + \mathrm{i}\lambda)}{2\eta} + \frac{(\eta - \mathrm{i}\lambda)}{2\eta}e^{2\mathrm{i}\eta t}.$$

Proof. Since M is a non-singular matrix, it can be verified that there exists a non-singular matrix Q such that

$$Q^{-1}MQ = N,$$

where

$$N = \begin{bmatrix} -\mathrm{i}\eta & 0 \\ 0 & \mathrm{i}\eta \end{bmatrix}, \quad Q = \begin{bmatrix} 1 & 1 \\ \mathrm{i}\eta & -\mathrm{i}\eta \end{bmatrix}, \quad \text{and} \quad Q^{-1} = \frac{1}{2\mathrm{i}\eta}\begin{bmatrix} \mathrm{i}\eta & 1 \\ \mathrm{i}\eta & -1 \end{bmatrix}.$$

A simple calculation yields that the fundamental matrix of (A.4)–(A.5) is

$$\Phi(y) = Q \begin{bmatrix} e^{\mathrm{i}\eta y} & \\ & e^{-\mathrm{i}\eta y} \end{bmatrix} Q^{-1},$$

which gives

$$\det \begin{bmatrix} A_0 \\ B_1\Phi(h) \end{bmatrix} = \begin{vmatrix} -\lambda & 1 \\ -\mathrm{i}\eta e^{-\mathrm{i}\eta h} & e^{-\mathrm{i}\eta h} \end{vmatrix} = (\mathrm{i}\eta - \lambda)e^{-\mathrm{i}\eta h} \neq 0 \quad \text{for } \lambda \neq \mathrm{i}\eta.$$

It follows from Theorem A.1 that the two-point boundary value problem (B.4)–(B.6) and thus (B.1)–(B.3) has a unique solution.

Let $\{A(y), r(y)\}$ and $\{B(y), s(y)\}$ be the integrated solutions of the problems (B.4), (B.5), and (B.4), (B.6), respectively. Taking

$$D_0 = \mathrm{i}\eta, \quad D_1 = -\mathrm{i}\eta,$$

we obtain from (A.7)–(A.10) that the integrated solutions satisfy

$$A' = AM + \mathrm{i}\eta A, \quad A(0) = A_0, \tag{B.8}$$

$$r' = A\mathbf{v} + \mathrm{i}\eta r, \quad r(0) = \phi, \tag{B.9}$$

and

$$B' = BM - \mathrm{i}\eta B, \quad B(h) = B_1, \tag{B.10}$$

$$s' = B\mathbf{v} - \mathrm{i}\eta s, \quad s(h) = \psi. \tag{B.11}$$

Upon solving the initial value problems (B.8) and (B.10), we obtain the integrated solutions for A and B:

$$A = [A_1(y)\ A_2(y)], \quad B = [B_1(y)\ B_2(y)], \tag{B.12}$$

where

$$A_1(y) = \frac{(\mathrm{i}\eta - \lambda)}{2} - \frac{(\mathrm{i}\eta + \lambda)}{2}\, e^{2\mathrm{i}\eta y}, \quad A_2(y) = \frac{(\eta + \mathrm{i}\lambda)}{2\eta} + \frac{(\eta - \mathrm{i}\lambda)}{2\eta}\, e^{2\mathrm{i}\eta y},$$

and

$$B_1(y) = -\mathrm{i}\eta, \quad B_2(y) = 1.$$

Once A and B are available, we may solve the initial value problems (B.9) and (B.11) and obtain the integrated solutions for r and s:

$$r(y) = e^{\mathrm{i}\eta y}\phi + \int_0^y e^{\mathrm{i}\eta(y-z)} A_2(z) v(z) dz, \tag{B.13}$$

$$s(y) = e^{\mathrm{i}\eta(h-y)}\psi - \int_y^h e^{\mathrm{i}\eta(z-y)} v(z) dz. \tag{B.14}$$

It follows from Theorem A.3 that the two-point boundary value problem (B.4)–(B.6) is equivalent to the linear system

$$\begin{bmatrix} A_1 & A_2 \\ B_1 & B_2 \end{bmatrix} \begin{bmatrix} u \\ u' \end{bmatrix} = \begin{bmatrix} r \\ s \end{bmatrix}.$$

An application of Gram's rule yields

$$u = \frac{rB_2 - sA_2}{A_1B_2 - B_1A_2}. \tag{B.15}$$

A simple calculation yields

$$A_1B_2 - B_1A_2 = \mathrm{i}\eta - \lambda.$$

Substituting (B.12)–(B.14) into (B.15), we deduce (B.7). □

REFERENCES

[1] H. Ammari, G. Bao, and A. Wood, *An integral equation method for the electromagnetic scattering from cavities*, Math. Meth. Appl. Sci., 23 (2000), pp. 1057-1072.

[2] I. Akduman, R. Kress, and A. Yapar, *Iterative reconstruction of dielectric rough surface profiles at fixed frequency*, Inverse Problems, 22 (2006), pp. 939–954.

[3] G. Bao, L. Cowsar, and W. Masters, *Mathematical modeling in optical science*, Frontiers in Applied Mathematics, vol. 22, SIAM, Philadelphia, 2001.

[4] G. Bao, D. Dobson, and J. A. Cox, *Mathematical studies in the rigorous grating theory*, J. Opt. Soc. Am. A, 12 (1995), pp. 1029–1042.

[5] G. Bao, J. Gao, and P. Li, *Analysis of direct and inverse cavity scattering problems*, Numer. Math. Theor. Meth. Appl., 4 (2011), pp. 419–442.

[6] G. Bao, P. Li, and H. Wu, *A computational inverse diffraction grating problem*, J. Opt. Soc. Am. A, 29 (2012), pp. 394–399.

[7] G. Bao, P. Li, and J. Lv, *Numerical solution of an inverse diffraction grating problem from phaseless data*, J. Opt. Soc. Am. A, 30 (2013), pp. 293–299.

[8] G. Bao and J. Lin, *Near-field imaging of the surface displacement on an infinite ground plane*, Inverse Probl. Imag., 7 (2013), pp. 377–396.

[9] O. Bruno and F. Reitich, *Numerical solution of diffraction problems: a method of variation of boundaries*, J. Opt. Soc. Am. A, 10 (1993), pp. 1168-1175.

[10] S. Carney and J. Schotland, *Inverse scattering for near-field microscopy*, App. Phys. Lett., 77 (2000), pp. 2798–2800.

[11] S. Carney and J. Schotland, *Near-field tomography*, MSRI Ser. Math. Appl., 47 (2003), pp. 133–168.

[12] S. N. Chandler-Wilde and P. Monk,*Existence, uniqueness and variational methods for scattering by unbounded rough surfaces*, SIAM J. Math. Anal., 37 (2005), pp. 598–618.

[13] S. N. Chandler-Wilde and B. Zhang, *A uniqueness result for scattering by infinite rough surfaces*, SIAM J. Appl. Math., 58 (1998), pp. 1774–1790.

[14] S. N. Chandler-Wilde, C. R. Ross, and B. Zhang, *Scattering by infinite one-dimensional rough surfaces*, Proc. Roy. Soc. London Ser. A, 455 (1999), pp. 3767-3787.

[15] Z. Chen and H. Wu, *An adaptive finite element method with perfectly matched absorbing layers for the wave scattering by periodic structures*, SIAM J. Numer. Anal., 41 (2003), pp. 799-826.

[16] R. Coifman, M. Goldberg, T. Hrycak, M. Israeli, and V. Rokhlin, *An improved operator expansion algorithm for direct and inverse scattering computations*, Waves Random Media, 9 (1999), pp. 441–457.

[17] D. Colton and R. Kress, *Inverse Acoustic and Electromagnetic Scattering Theory*, Applied Mathematical Sciences, vol. 93, Springer-Verlag, Berlin, 1998.

[18] D. Courjon, *Near-Field Microscopy and Near-Field Optics*, Imperial College Press, London, 2003.

[19] D. Courjon and C. Bainier, *Near field microscopy and near field optics*, Rep. Prog. Phys., 57 (1994), pp. 989-1028.

[20] J. A. DeSanto and P. A. Martin, *On the derivation of boundary integral equations for scattering by an infinite one-dimensional rough surface*, J. Acoust. Soc. Am., 102 (1997), pp. 67-77.

[21] J. A. DeSanto and R. J. Wombell, *The reconstruction of shallow rough-surface profiles from scattered field data*, Inverse Problems, 7 (1991), pp. L7–L12.

[22] H. Engl, M. Hanke, and A. Neubauer, *Regularization of Inverse Problems*, Kluwer Academic Publishers, Dordrecht, 1996.

[23] C. Girard and A. Dereux, *Near-field optics theories*, Rep. Prog. Phys., 59 (1996), pp. 657-699.

[24] J. Jin, *The Finite Element Method in Electromagnetics*, Wiley & Sons, New York, 2002
[25] R. Kress and T. Tran, *Inverse scattering for a locally perturbed half-plane*, Inverse Problems, 16 (2000), pp. 1541–1559.
[26] P. Li and J. Shen, *Analysis of the scattering by an unbounded rough surface*, Math. Meth. Appl. Sci., 35 (2012), pp. 2166–2184.
[27] P. Li and A. Wood, *A two-dimensional Helmholtz equation solution for the multiple cavity scattering problem*, J. Comput. Phys., 240 (2013), pp. 100–120.
[28] P. Li, H. Wu, and W. Zheng, *Electromagnetic scattering by unbounded rough surfaces*, SIAM J. Math. Anal., 43 (2011), pp. 1205-1231.
[29] C. D. Lines and S. N. Chandler-Wilde, *A time domain point source method for inverse scattering by rough surfaces*, Computing, 75 (2005), pp. 157–180.
[30] A. Malcolm and D. P. Nicholls, *A field expansions method for scattering by periodic multilayered media*, J. Acout. Soc. Am., 129 (2011), pp. 1783–1793.
[31] A. Malcolm and D. P. Nicholls, *A boundary perturbation method for recovering interface shapes in layered media*, Inverse Problems, 27 (2011), 095009.
[32] D. M. Milder, *An improved formalism for wave scattering from rough surfaces*, J. Acoust. Soc. Am., 89 (1991), pp. 529–541.
[33] D. P. Nicholls and F. Reitich, *Shape deformations in rough surface scattering: cancellations, conditioning, and convergence*, J. Opt. Soc. Am. A, 21 (2004), pp. 590-605.
[34] D. P. Nicholls and F. Reitich, *Shape deformations in rough surface scattering: improved algorithms*, J. Opt. Soc. Am. A, 21 (2004), pp. 606-621.
[35] P. Persson and G. Strang, *A Simple Mesh Generator in MATLAB*, SIAM Review, 46 (2004), pp. 329–345.
[36] A. G. Voronovich, *Wave Scattering from Rough Surfaces*, Springer, Berlin, 1994.
[37] K. Warnick and W. C. Chew, *Numerical simulation methods for rough surface scattering*, Waves Random Media, 11 (2001), pp. R1-R30.
[38] B. Zhang and S. N. Chandler-Wilde, *Acoustic scattering by an inhomogeneous layer on a rigid plate*, SIAM. J. Appl. Math., 58 (1998), pp. 1931–1950.
[39] B. Zhang and S. N. Chandler-Wilde, *Integral equation methods for scattering by infinite rough surfaces*, Math. Meth. in Appl. Sci., 26 (2003), pp. 463–488.
[40] G.-Q. Zhang, *Integrated solutions of ordinary differential equation system and two-point boundary value problems, I. Integrated solution method*, J. Comp. Math., 3 (1981), pp. 245–254.